MJFAS
Malaysian Journal of Fundamental and Applied Sciences

Alakbaree *et al.* | Malaysian Journal of Fundamental and Applied Sciences, Vol. 20 (2024) 1440-1459

RESEARCH ARTICLE

Understanding Acute Hemolytic Anemia Severity Through Computational Analysis of G6PD^{Chatham} Variant: Designing a New Activator as a Potential Drug

Maysaa Alakbaree[a], Mustapha Suleiman[b], Abbas Hashim Abdulsalam[c], Ahmed Al-Hili[d], Mohd Shahir Shamsir Omar[e], Farah Hasan Ali[f], Nurriza Ab Latif[e], Muaawia Ahmed Hamza[g], Syazwani Itri Amran[e*]

[a]Department of Bioinformatics, College of Biomedical Informatics, University of Information Technology and Communications, Baghdad, Iraq; [b]Department of Chemistry, Faculty of Science, Universiti Teknologi Malaysia, 81310 UTM Johor, Malaysia; [c]Department of Medical Laboratories Techniques, Al-Turath University College, Baghdad, Iraq; [d]Department of Anesthesia, Collage of Medical Technology, Al-Farahidi University, Baghdad, Iraq; [e]Department of Biosciences, Faculty of Science, Universiti Teknologi Malaysia, 81310 UTM Johor, Malaysia; [f]Department of Radiology and Ultrasound, Collage of Medical Technology, Al-Farahidi University, Baghdad, Iraq; [g]Faculty of Medicine, King Fahad Medical City, Research Center, King Fahad Medical City, Riyadh, Saudi Arabia

Abstract Glucose-6-phosphate dehydrogenase deficiency (G6PDD) is a major enzymatic disease affecting human red blood cells (RBCs), causing hemolytic anemia due to the diminish of the nicotinamide adenine dinucleotide phosphate hydrogen (NADPH) synthesis and altered redox balance within erythrocytes. This study sought to correct the defect in G6PD^{Chatham} (Ala355Thr) caused by the loss of interactions (hydrogen bonds and salt bridges) by docking the AG1 molecule at the dimer interface, thus restoring these lost interactions. The enzyme conformation was then analyzed before and after AG1 binding using molecular dynamics simulation (MDS). The reasons behind the severity of acute hemolytic anemia (AHA) were explained using several parameters, such as root-mean-square deviation (RMSD), root-mean-square fluctuation (RMSF), hydrogen bonds, salt bridges, radius of gyration (Rg), solvent accessible surface area (SASA), and covariance matrix analysis. Structural alterations in G6PD^{Chatham}, including the absence of interactions in a key region of the variant structure, can significantly impact protein stability and function, subsequently contributing to disease severity. Upon AG1 binding, these missing interactions were resorted to correct the structural defect of the variant. This restoration improves dimer stability and restores G6PD function. To develop new G6PD activators, several new analogues (SY7, SY8, SY9, and SY10) were rationally developed by substituting the linker region of the AG1 structure with other functional groups using the Avogadro software. These compounds were successfully synthesized and docked with G6PD^{Chatham} where the best binding affinity ranged between -8.0 and -9.1 kcal/mol. SY8, a promising G6PD activator, is predicted to be easily metabolized and excreted, making it less likely to cause toxicity. Its high drug score, drug-likeness, and favorable safety profile make it a strong candidate for synthesis and cellular testing. The toxicity risk assessment supported the overall drug score, increasing confidence in finding additional small-molecule activators for G6PDD disorder. Amidst the absence of effective treatments, such discovery hopes to improve the lives of those with AHA by assisting the development of appropriate pharmaceuticals for G6PDD.

Keywords: C6PD^{Chatham}, molecular dynamic simulation, molecular docking, acute hemolytic anemia, computer-aided drug design.

***For correspondence:**
syazwaniitri@utm.my

Received: 21 Sept. 2024
Accepted: 04 Nov. 2024

Introduction

Glucose-6-phosphate dehydrogenase (G6PD) is an essential enzyme that exists on the X chromosome. It activates the pentose phosphate pathway (PPP) and produces NADPH, which is required for regulating oxidative stress (OS) in red blood cells (RBCs). Without G6PD, cells cannot create NADPH and are susceptible to oxidative damage, resulting in cell death [1]. According to [2], the G6PD gene contains OMIM ID 305900 and spans 18 kilobases on the X chromosome at the Xq28 location. It also consists of a 1,545 base-pair open reading frame (ORF) that encodes 515 amino acids. To date, approximately 217 mutations of this gene have been reported globally [2].

Past studies have reported that the lack of the G6PD enzyme may cause the cell membrane to rupture abnormally and result in hemolytic anemia [3]. Such condition is commonly known as G6PD deficiency (G6PDD) and is caused by hereditary defects in the G6PD gene [4]. Furthermore, G6PDD is associated with episodic hemolytic anemia (induced by fava beans or other stimuli) or lifelong hemolytic anemia [5]. This might develop into transfusion-required acute hemolytic anemia every year [6]. Recent statistics show that G6PDD affects more than 500 million individuals globally [7]. Interestingly, it has a notably high incidence rate in the Arab countries: up to 39.8% in Saudi Arabia, 30% in Syria, 29% in Oman [8, 9], 3.6% in Jordan, 5% in Baghdad, and 10% in Kuwait [10]. Following the $G6PD^{Mediterranean}$ [Ser188Phe] variant, $G6PD^{Chatham}$ is the most prevalent variant in many Middle Eastern countries [3]. Nevertheless, no research has been conducted to study the molecular structure of $G6PD^{Chatham}$ and its functional role in creating the illness, alongside the causes for its severity, particularly in Arab countries.

Despite the 230 mutations recorded worldwide [7], only 10% of G6PD variants have been studied at the molecular and functional levels and how they relate to clinical symptoms [11, 12]. The World Health Organization (WHO) classifies G6PDD into four categories based on median G6PD activity and hemolysis. Class A is defined by less than 20% of G6PD activity, resulting in chronic hemolysis known as chronic non-spherocytic hemolytic anemia (CNSHA). Individuals with less than 45% of G6PD activity are classified as Class B, with acute hemolysis triggered by specific factors. Class C has G6PD activity ranging from 60% to 150% with no chances of developing hemolysis. Finally, Class U refers to any level of G6PD activity with unknown clinical implications concerning hemolysis [7].

Understanding the structural-functional relationship for G6PD variants can be challenging since many mutations are distributed throughout the protein structure [13]. Furthermore, the substitution of several amino acids *in vitro* is expensive and time-consuming. In contrast, a comprehensive analysis that involves a systematic modification of all amino acids in the protein is impossible; hence, computational methods have been developed to predict the effects of mutations [14]. This highlights the imperative need to understand the molecular mechanisms of the disease's severity. Because G6PD is expressed by a number of hematologic and nonhematologic cells, patients with G6PDD can develop a broader range of clinical symptoms [15]. Moreover, G6PDD is characterized by elevated oxidative stress levels, which can affect various physiological processes and illness consequences. The impact of G6PDD may also extend to different medical disorders, such as viral infections, cancer, hypertension, asthma, Alzheimer's disease, acute kidney injury, diabetes, ischemic priapism, and severe hemolysis [16].

Despite the prevalence of G6PDD and its association with mild to severe and chronic hemolytic anemia, no therapies currently exist. The severe form of G6PDD is CNSHA, which could be treated by allogeneic bone marrow transplantation or gene therapy; however, this has yet been attempted to date [17]. A study by [18] highlighted the effects of AG1, a small molecule that increased G6PD enzyme activity. They observed that AG1 enhanced activation by stabilizing the dimeric state of various G6PD enzyme variants. The molecule also increased G6PD oligomerization, which might provide a first-in-class therapy for G6PDD. This generic technique might be useful to treat additional enzyme deficits where oligomerization can improve enzymatic activity and/or stability [18]. Furthermore, an earlier computational prediction discovered that the disulfide linker presence in the AG1 molecule is unnecessary for activation [19].

Therefore, this work attempts to develop new G6PD activators using the AG1 molecule as a template. It was achieved by substituting the inactive disulfide linker with several functional groups using computer-aided drug design (CADD). Past studies denote that CADD is a powerful technique for facilitating therapeutic development [20]. Such technique not only contributes to cost reduction in drug discovery but also has the potential to accelerate the time for a drug to reach the market [21]. Nowadays, CADD approaches like molecular docking and MDS are widely used to discover, develop, and analyze drugs of similar biologically active molecules [22]. Determining the binding capacity of a compound is typically time-consuming and costly in traditional drug development as it requires extensive *in vitro* and *in vivo* experiments. Conversely, the use of molecular docking offers a faster and more accessible alternative.

This study focused mainly on the CADD process to identify a new activator molecule that could potentially tackle the health issues associated with different G6PDD variants. Achieving the optimal drug discovery method may be challenging; yet, establishing a paradigm that integrates rational drug discovery with a robust focus on physiology and disease can be straightforward [23]. The objective of this study is to uncover the molecular mechanisms underlying the severe acute hemolytic anemia (AHA) caused by Class B ($G6PD^{Chatham}$ [Ala335Thr]) mutation by employing bioinformatics methodologies. Traditional biochemical analyses of such variants face difficulties in obtaining sufficient pure protein due to the enzyme's high instability [24]. Furthermore, only a limited number of G6PD mutations have been investigated using computational approaches [25]. Experimental investigation for each mutation is also impractical due to the vast array of G6PD mutations; however, computational methods offer a promising avenue to predict and assess the impact of numerous mutations. Therefore, another objective of this study is to elucidate the molecular basis of the chosen mutation's pathogenicity by utilizing bioinformatics tools, hoping to better comprehend its role in severe acute hemolytic anemia. This study also compares the mutation before and after AG1 binding to better understand how mutations impact variant structure and how the AG1 molecule improves stability in $G6PD^{Chatham}$. Such insights will facilitate the designing of new activators to fight G6PDD, which may be used as a new therapy for AHA.

Materials and Methods

In Silico Site Directed Mutagenesis

A complete G6PD dimer structure in complex with G6P substrate and $NADP^+$ cofactors in both chains was built according to a previously published procedure [26]. *In silico* site-directed mutagenesis was done using the PyMOL Molecular Graphics System version 2.5.2 to produce $G6PD^{Chatham}$ (Ala335Thr). The PDB file for the selected variant was uploaded into PyMOL and the sequence and residue options were chosen using the display button in the PyMOL viewing window. Next, the sequences for Chains A and B were displayed and the mutagenesis option was selected from the wizard menu, followed by the protein choice. A new window later appeared and the 'no mutation' option was selected. Conversely, the resulting residue was picked, and the amino acid was altered according to the selected variant (Ala335Thr). After applying these parameters, the file was saved as a PDB.

Molecular Docking

The small molecule activator (AG1) was retrieved from PubChem (https://pubchem.ncbi.nlm.nih.gov/compound/6615809) an open chemistry database, includes chemical information that used for virtual screening. PubChem's data integration with DrugBank provides extensive information on FDA-approved and experimental medications [27]. The G6PD mutant structure underwent a preparation phase where water molecules were eliminated and saved in .pdb format. The PyRx software (https://pyrx.sourceforge.io) a virtual screening tool is a computational drug discovery program that can evaluate libraries of compounds against possible therapeutic targets [27] was used to add the polar hydrogen atoms and partial charges, which is a crucial step for computing the electrostatic energy component [28]. A geometry optimization process was applied to the AG1 ligand ($C_{24}H_{30}N_4S_2$; N, N'-[disulfanediyldi(ethane-2,1-diyl)] bis[2-(1H-indol-3-yl) ethan-1-amine]), which was retrieved from PubChem (CID: 6615809) via energy minimization (EM). The optimized ligands were saved in .pdb format [29, 30]. A grid box was formed at the centroid of the protein's dimer interface and proximate to Asp421 and Glu419 [18, 31]. The coordinates for the grid center points were defined as (X = 16.83, Y = 100.82, and Z = 19.05). Typically, the exploration of different molecular conformations is accomplished via a Lamarkian genetic algorithm to assess how ligands interact with a specific protein [32]. The docking technique was done at least five times to acquire the best conformations. The docking results were assessed by evaluating the free binding energy values, the ligands binding interactions, and superimposition with the variant structure. To validate the protein-ligand interactions, Discovery Studio Visualizer (DSV) 4.0 was used to determine the favorable intermolecular interactions, such as hydrogen bonds and hydrophobic contacts [33]. This analysis aims to provide insights into the specific molecular associations between the ligand and the binding site, elucidating the nature of interactions critical for understanding the ligand's binding mechanism and stability [34].

Molecular Dynamic Simulation (MDS)

The simulations were conducted in two phases: before and after binding to the AG1 activator compared to $G6PD^{WT}$ for a duration of 100 ns using the GROMACS 2018.8 package [35]. The purpose of these simulations was to assess the stability of the complex structure and investigate the effects of AG1 on the variant's structure. Protein preparation was conducted by utilizing the pdb2gmx utility with the GROMOS 96 54a7 force field [36]. The use of the GROMOS96 54a7 force field aimed to enhance helical characteristics and improve hydration-free energy as well as improper dihedrals [35]. The AG1 molecule

was submitted to the PRODRG website a tool that generates molecular topologies and unique molecular descriptors from small molecules' coordinates to undergo ligand preparation and generate the necessary topology files for simulation [37]. The formation of the protein-ligand complex involved combining the ligands' atomic coordinates with those of the protein and updating both the protein's topology (.topol) and atomic coordinates (.gro). Every system was housed in a cube-shaped box with the following dimensions: (X: 8.976, Y: 11.412, and Z: 8.233) nm, a box angle of 90.00 degrees, and a box volume of 3018.13 nm^3. The system was solvated using simple point-charge (SPC) water molecules and the charge was neutralized by introducing an appropriate amount of sodium ions using GROMACS's genion module. All systems were subjected to energy optimization until they reached a value of 1000 kJ. They later underwent temperature equilibration at a consistent 300 K through a two-step ensemble process, namely the NVT (constant Number of particles, Volume, and Temperature) stage and NPT (constant Number of particles, Pressure, and Temperature) stage [38], each lasting for 100 ps. During the NVT stage, Berendsen thermostats were employed with no pressure coupling. Whereas, the Parrinello-Rahman method was applied in the NPT ensemble to maintain a pressure of 1 bar (P), ensuring system stability [39, 40]. Various analyses were conducted to assess different aspects of the protein's behavior during the simulation, including RMSD, RMSF, hydrogen bonds, salt bridges, RG, SASA, and covariance matrix.

Designing a New Activator Molecule and Molecular Docking

The AG1 structure's linker region was modified by substituting it with various functional groups using the Avogadro software (http://avogadro.cc/) a cross-platform molecule editor and visualizer which enables the development and study of molecular structures [41].The AG1.pdb file was loaded into the Avogadro molecular editor for structural modification. Hydrogen atoms were removed using the built-in tool with the 'Adjust Hydrogens' option turned off to avoid accidental hydrogen addition during further adjustments. The ligand structure was targeted by substituting functional groups at preset places. Following alteration, the ligand was energy optimized using the geometry optimization tool in Avogadro. This iterative technique sought to attain the lowest energy state while maintaining structural stability and conformational integrity. Each candidate compound was docked and analyzed as previously described in the molecular docking section.

Pharmacokinetic and Toxicity Risks Assessment

The drug-like properties and pharmacokinetic characteristics, including absorption, distribution, metabolism, and excretion (ADME), were evaluated using the SwissADME server (http://www.swissadme.ch/about.php), It's an open-access and rapid prediction models that exhibited statistical significance, predictive strength, intuitive interpretation, and easy translation to molecular design [42]. For the SwissADME analysis, the chemical structures were uploaded to the SwissADME online service using a Simplified Molecular Input Line Entry System (SMILES) format. After hitting the "Run" button, automatic analysis began effortlessly. This thorough investigation included an assessment of critical factors, such as lipophilicity, water solubility, pharmacokinetics, druglikeness, and medicinal chemistry. Furthermore, it evaluated drug-likeness using recognized criteria, such as Lipinski's Rule of Five. The analysis produced extensive reports that were created automatically and summarized all findings. Visual representations in the form of 2D and 3D structural views were also provided to help with reading comprehension. Likewise, Osiris molecular property explorer (https://www.organic-chemistry.org/prog/peo/) calculated several drug-relevant characteristics and displayed a variety of properties important to pharmaceuticals and chemical substances [43]. These included molecular weight and LogP (Logarithm of the Partition Coefficient) that measures a compound's solubility in a hydrophobic solvent relative to water. A higher Log P value implies more hydrophobicity and solubility in non-polar solvents, whereas a lower value indicates enhanced water solubility. This feature is significant in drug design and pharmacokinetics, since it affects drug absorption, distribution, metabolism, and excretion (ADME) [43]. The program also forecasted water solubility, analyzed drug-likeness using usual pharmacological features, and examined mutagenicity and carcinogenicity concerns. It also offered a therapeutic score, which combined many factors to assess a compound's potential as a therapeutic candidate. Prediction findings were rated and color-coded as red (properties with a significant risk of adverse implications, such as mutagenicity or poor intestinal absorption) or green (drug-compliant behavior) [42]. The analysis began with the OSIRIS Property Explorer's web-based interface where the chemical structure was entered by uploading a file in SMILES format to ensure conformity with chemical regulations via the program's automated validation. This step ensured that errors due to incorrect structures were avoided. Once approved, the OSIRIS Property Explorer computed important characteristics automatically. The examined data was then stored or exported in various forms for future recording and study. Based on the attributes and assessments gathered, educated conclusions were made regarding the compound's potential for medication development.

Results and Discussion

Conformational Alterations Caused by Mutations

G6PD^{Chatham} (Ala335Thr) was found in the loop of the G6PD structure between Thr311 and Thr336 [44]. This mutation was generated by replacing guanine with adenine (G → A) in nucleotide (nt) 1003 (exon 9) which led to a change of alanine (Ala) with threonine (Thr) at position 335, resulting in severe hemolytic anemia [45]. Following the replacement of Ala335 with Thr in both Chains A and B, prominent instances of new hydrogen bonds were formed with residues Phe337 and Gly306 (see Figure 1). These hydrogen bonds indicated major structural changes inside the protein, which might affect its stability and functional dynamics. Additionally, the close proximity of G6PD^{Chatham} to the G6P binding site (~ 10 Å) may impact its binding while the mutation of Ala at position 335 by the Thr residue altered the loop's conformation (residues Thr311–Thr336). The bigger side chain in Thr also allowed hydrogen bond formation with nearby residues, such as Phe337 and Gly306, while maintaining hydrogen bond interactions with Ile255 (see Figure 1). The substitution amino acid that does not fit into the protein may cause structural changes that are usually deleterious [46]. Additionally, mutations can affect the G6PD enzyme's local and global stability by altering the characteristics of the mutant amino acids or their interactions (loss, increase, or reduction in distance) [47].

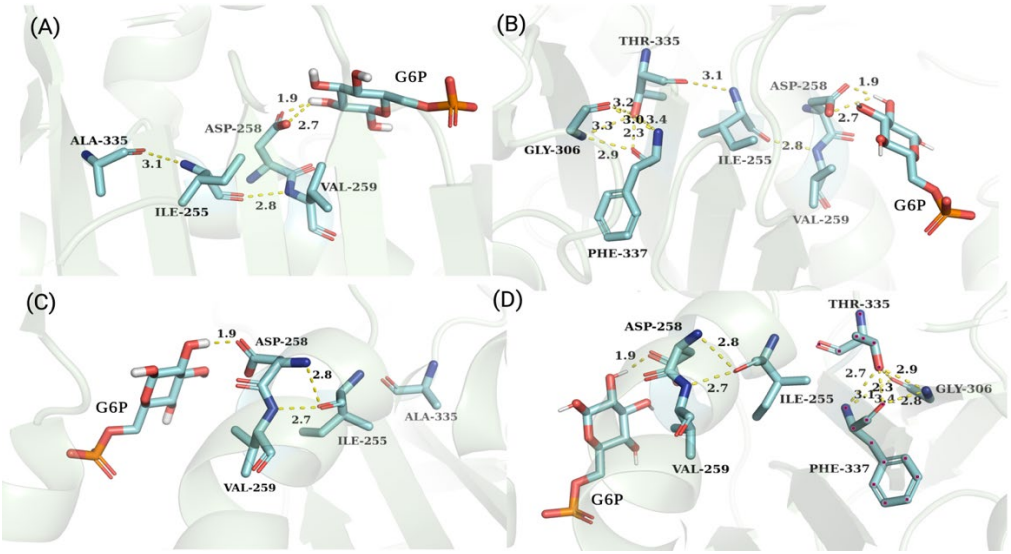

Figure 1. The G6PD^{WT} and G6PD^{Chatham} interactions with the Ala335 residue and its mutation. Chain A contains (a) the native amino acid Ala335 and (b) the mutant amino acid Thr335. Chain B contains (c) native amino Ala335 and (d) mutant amino acid Thr335

Molecular Docking

Recent advances in computational docking simulations allow for a fast, cost-effective, and extensive study of protein-ligand interactions using computer-based (*in silico*) approaches [48]. Following the preparation of the variant structure and ligand (AG1), G6PD^{Chatham} had AG1 docked at the dimer interface. Similarly, attempts to dock this molecule in other important areas (e.g., catalytic $NADP^+$ binding site, G6P substrate, and tetramer area) led to no effects, although the binding of AG1 was observed at these positions. This implies that the chosen variant might possess a distinctive binding mechanism or that the docking of AG1 at the dimer interface is crucial for its functionality [19].

Analysis of the Docking Results

PyRx is a virtual screening tool that employs the advanced features of AutoDock Vina to dock analogous molecules into G6PD^{Chatham}. The binding affinity of AG1 to G6PD^{Chatham} variant was (-7.1) kcal/mol. The DSV tool was utilized to evaluate the protein-ligand docking results [49]. Figure 2 and Table 1 illustrate the interactions after AG1 bindings. Based on the previous computational prediction [19], the activation mechanism does not involve disulfide group located at the center of AG1. Hence, different functional groups were proposed at this site.

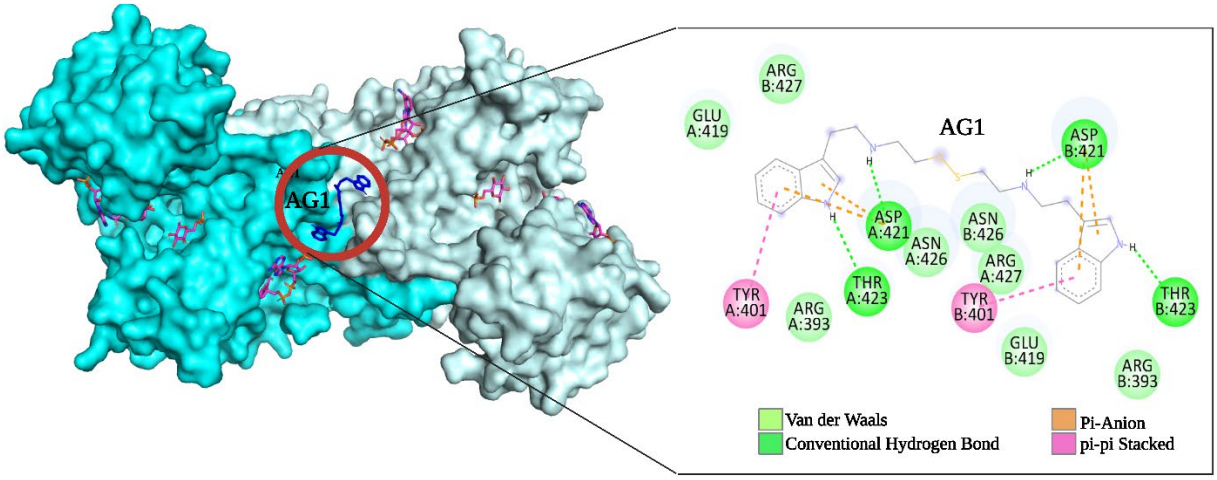

Figure 2. Docking analysis of G6PD^{Chatham_AG1}. Left - the G6PD dimer structure is depicted in surface representation: Chain A (dark cyan); Chain B (light cyan); the ligands (catalytic NADP$^+$, G6P, and structural NADP$^+$) are depicted as pink sticks; and AG1 is represented as a blue stick. Right - AG1 molecule is represented in a 2D line model. Interactions are depicted as dashed lines with circles highlighting the amino acids involved

Table 1. Amino acids interacted with the AG1 molecule following the G6PD^{Chatham} docking process

Interactions	Amino Acids	Chains
Van der Waals	Arg393 - A	A
	Asn426 - A	A
	Arg427 - A	A
	Glu419 - A	A
	Asn426 - B	B
	Glu419 - B	B
	Arg393 - B	B
	Arg427 - B	B
Conventional hydrogen bonds	Thr423 - A	A
	Asp421 - A	A
	Thr423 - B	B
	Asp421 - B	B
Pi - Anion	Asp421 - A	A
	Asp421 - B	B
pi-pi Stacked	Tyr401 - A	A
	Tyr401 - B	B

Post Trajectory Analysis of MDS

This study utilized the MDS approach to create trajectories for understanding the folding/unfolding properties and protein conformation represented by various properties, including RMSD, RMSF, Hydrogen bond number, salt bridges analysis, covariance matrix, Rg, and SASA.

Root Mean Square Deviation (RMSD)

The RMSD value was calculated to examine the convergence of trajectory files and measure the degree to which the protein structure shifted throughout the simulation process [50]. The stability of G6PD^{WT} and G6PD^{Chatham} was evaluated using RMSD values, which were plotted as a function of time. Figure 3a shows the RMSD value over 100 ns. Before binding to AG1, G6PD^{Chatham} exhibited RMSD values ranging from 0.21 to 0.54 nm with an average of 0.34 nm. Minor deviations were noted at 11, 20, and 31 ns. Subsequently, there was a decrease in RMSD value at 41 ns, followed by a sudden increase at 49 ns and a decrease at 58 ns before maintaining a constant value until the simulation ended. The higher

deviations in RMSD values exhibited by G6PD^{Chatham} compared to G6PD^{WT} signify reduced structural stability. Given that a stable structure is crucial for the proper functioning of the protein, these findings underscore how mutations can significantly impact the stability and G6PD enzyme activity. It subsequently highlights the importance of understanding these structural dynamics in the context of clinical implications. Conversely, additional parameters must be examined to investigate potential contributing factors to the alteration in stability [51].

A significant impact on conformational stability was observed in G6PD^{Chatham_AG1} complex. The AG1 activator led to a decrease in RMSD value to 0.25 nm (Figure 3b). In simpler terms, the selected variant displayed significantly improved overall stability compared to G6PD^{WT}. Such improvement in structural stability is believed to result from the AG1 activator enhancing dimer stabilization, thus restoring enzyme activity [19].

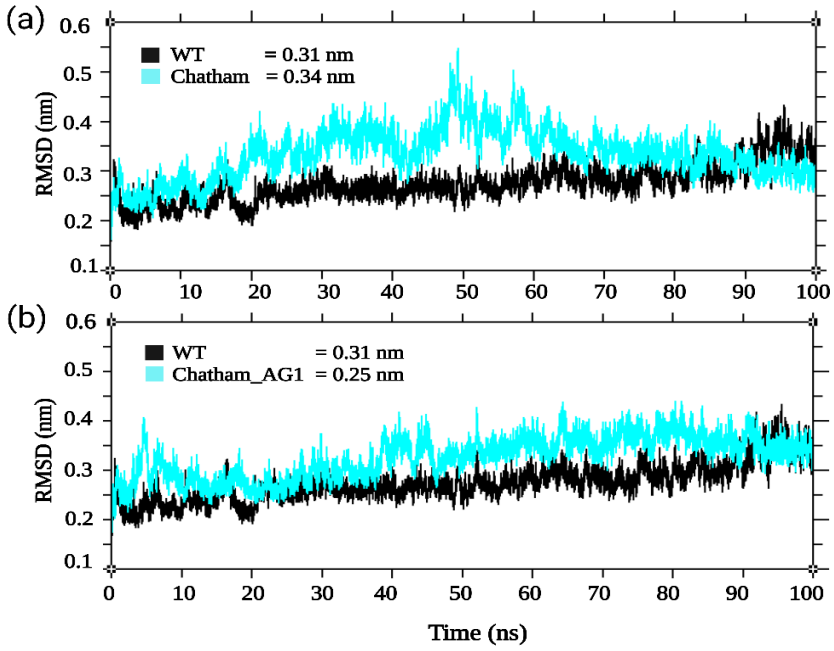

Figure 3. RMSD of the protein backbone, G6PD^{Chatham}, against G6PD^{WT} in the absence and presence of AG1 molecule at 100 ns simulation

Root Mean Square Fluctuation (RMSF)

The RMSF analysis was conducted to compare the flexibility of each residue in G6PD^{Chatham} against the WT enzyme in the presence and absence of AG1 at 100 ns trajectory (see Figure 4 and Table 1). Although the G6PD enzyme dimer comprised two identical monomers, the two chains behaved differently. As demonstrated in Figure 4 (a and b), Chain B had a larger RMSF value than Chain A, which was clearly evident in the variant structure. As shown in Table 2, Figure 5 (a and b), and Figure 6 (a, b, c, d, e, and f), structural loops at key locations, such as structural $NADP^+$ binding site, G6P substrate binding site, and dimer interface, demonstrated higher flexibility. This suggests a relationship between RMSF and the quantity of intermolecular hydrogen bonds, with higher RMSF values are associated with a reduced total count of intermolecular hydrogen bonds. Notably, substantial fluctuations in G6PD^{Chatham} can be accounted to loss of hydrogen bonds, affecting the enzyme structural stability (see Figure 1). Interestingly, the selected variant showed reduced flexibility after AG1 binding, as shown in Table 2, Figure 5 (c and d), and Figure 6 (g, h, i, j, k, and l).

A thorough observation of these results indicates that G6PD^{Chatham} demonstrated a significant degree of flexibility. Such mutation increased the protein's flexibility of the variant compared to G6PD^{WT}. Moreover, the RMSF values were consistent with RMSD. High RMSD values in variant structure may indicate considerable structural alterations or deviations, implying possible conformational instability. These alterations can be attributed to various reasons, including the flexibility or mobility of certain areas within the protein and possible structural rearrangements. Therefore, both RMSD and RMSF stand as valuable indicators for assessing protein stability and flexibility in MDS analysis .

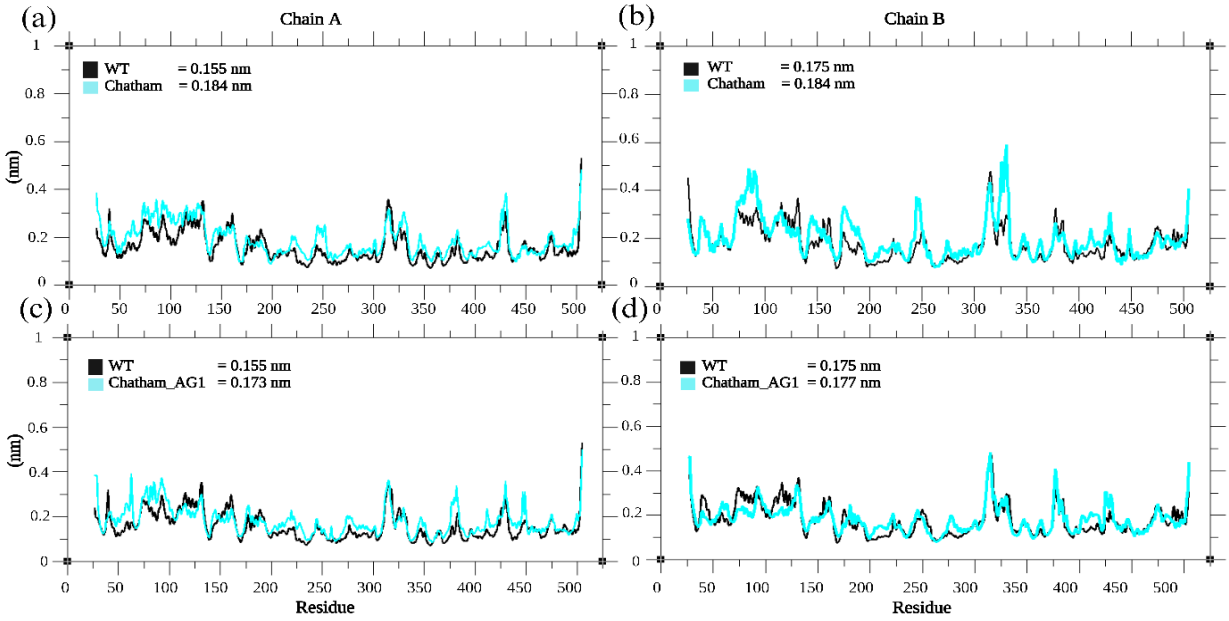

Figure 4. The RMSF analysis of G6PD^{Chatham} (cyan) over G6PD^{WT} (black) in both Chains A and B during 100 ns simulation in the absence (a – b) and presence (c – d) of AG1 demonstrated similar amino acid fluctuation pattern between G6PD$^{Chatham-AG1}$ and G6PD^{WT}

Table 2. RMSF at crucial locations in the selected variants was assessed after interaction with the AG1 molecule

Residue Fluctuation Range	RMSF (nm)	Protein Region	Figures
Chain A - G6PD^{Chatham}			
430 – 432	Val431 = 0.286	Dimer interface	5a & 5b
Chain B - G6PD^{Chatham}			
409 – 413	Met411 = 0.240	Dimer interface	6a & 6b
243 - 250	Gly245 = 0.372	G6P substrate	6c & 6d
361 – 365	Asn363 = 0.197	Structural NADP$^+$	6e & 6f
G6PD^{Chatham} –AG1 (Chain A)			
430 – 432	Val431 = 0.286	Dimer interface	5c & 5d – (c and d)
G6PD^{Chatham} –AG1 (Chain B)			
409 – 413	Met411 = 0.200	Dimer interface	6g & 6h – (g and h)
243 - 250	Gly245 = 0.215	G6P substrate	6i & 6j – (i and j)
361 – 365	Asn363 = 0.176	Structural NADP$^+$	6k & 6l – (k and l)

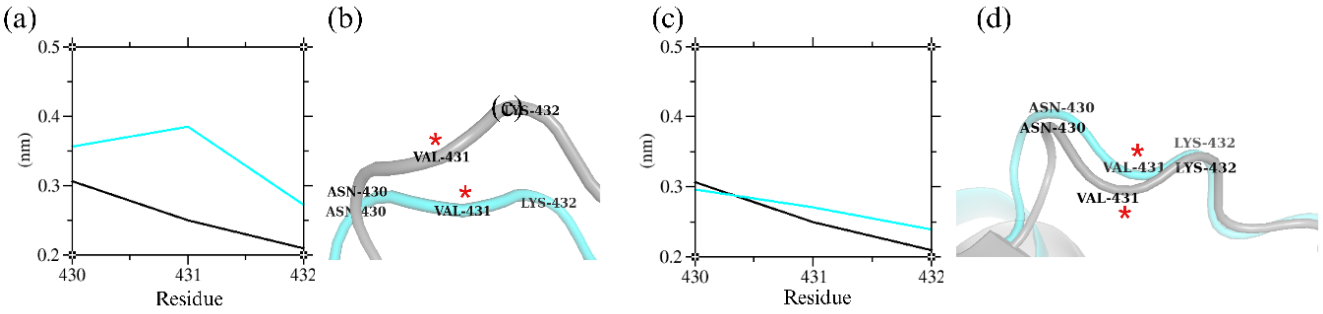

Figure 5. The RMSF of G6PD^{Chatham} (cyan) in comparison to G6PD^{WT} (grey) in both Chains A and B. The fluctuation regions are depicted in a 2D plot. Before AG1 binding: (a) between (430 – 432). After AG1 binding: (b) between (430 – 432). The PyMOL visualization [(b) and (d)] illustrates fluctuations in the same regions for residues represented by the cartoon. Significant areas with high residue levels are marked with red stars

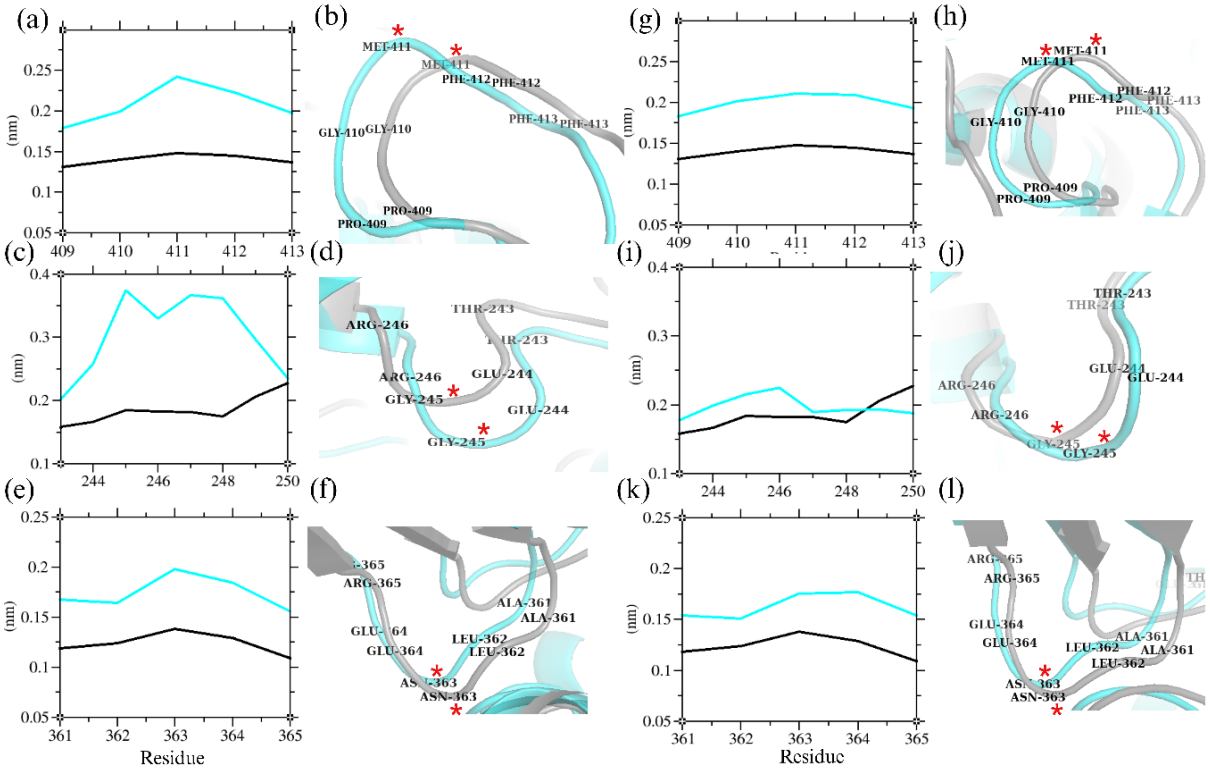

Figure 6. The RMSF of G6PDChatham (cyan) compared to G6PDWT (grey) for both Chains A and B is shown in a 2D plot. Fluctuation areas prior to AG1 binding are noted at residues 409-413 (a), 244-250 (c), and 361-365 (e). Following AG1 binding, variations occur in the same regions: 409-413 (g), 244-250 (i), and 361-365 (k). The PyMOL visualization illustrates these fluctuations, with residues represented by cartoons: before AG1 binding (b, d, f) and after AG1 binding (h, j, l). Significant areas with high residue fluctuations are marked with red stars

Hydrogen Bonds and Salt Bridges

To gain further insights into previous findings, an analysis was conducted on the number of hydrogen bonds formed within G6PD^{WT} and the selected variant over time. The preservation of protein conformation primarily relies on hydrogen bonding while the flexibility of the protein is directly influenced by the intramolecular hydrogen bonds formed between amino acid residues [52]. As shown in Figure 7a, G6PD^{Chatham} has lower hydrogen bonds than G6PD^{WT} with 794.722 and 825.141, respectively. This implies that the variant lost a considerable amount of hydrogen bonds, which reduced protein compactness and resulted in a less stable structure compared to G6PD^{WT}. Furthermore, this mutation might affect the G6P substrate and $NADP^+$ cofactors affinity impacting the enzyme's activity. These findings are similar to Sukumar *et al*. (2003) [53] who reported that the G6PD^{Chatham} variant is associated with considerable low enzyme activity. Following AG1 binding, the hydrogen bonds in G6PD^{Chatham} increased to 812.760 compared to G6PD^{WT} (825.141) and G6PD^{Chatham} (794.722) (see Figure 7b).

The dimer interface of the G6PD structure relies on four salt bridges: Glu206 with Lys407 and Glu419 with Arg427 [54]. Salt bridges play a crucial role in various protein functions, such as molecular recognition, degradation, allosteric regulation, domain movements, and flexibility, thermostability, and can be either stabilizing or destabilizing [55, 56, 57]. The breakdown and insertion of a salt bridge can lower and improve protein stability, respectively [55]. These interactions involve attractive forces between oppositely charged amino acid residues and are essential for maintaining the overall structure and function of proteins. In G6PD^{Chatham}, one salt bridge was lost between Glu419 and Arg427. However, the identical salt bridge interaction was restored when it was complexed with AG1 (G6PD$^{Chatham\text{-}AG1}$). These findings demonstrate that AG1 aids in the repair of missing contacts, implying corrective effects on structural integrity. Therefore, it can be concluded that G6PD^{WT} has the highest number of hydrogen bonds and salt bridges than the mutant enzyme, rendering it more stable relatively. The occurrence of the selected variant led to the loss of a large number of hydrogen bonds and subsequently decreased protein stability [58]. Meanwhile, G6PD^{Chatham} has the lowest stability concerning G6PD^{WT}.

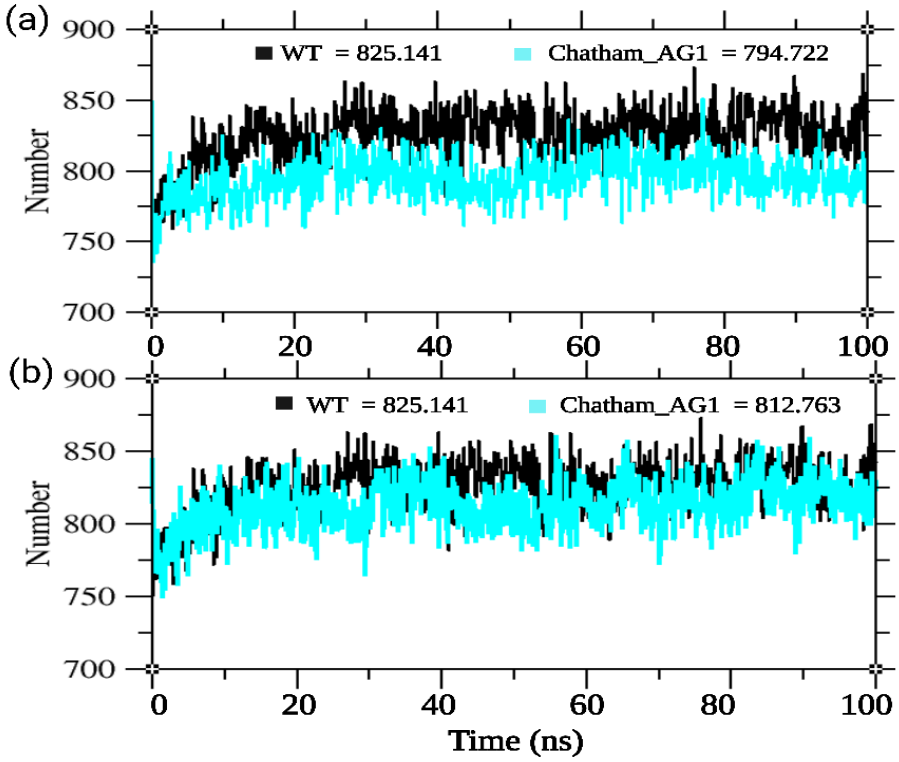

Figure 7. H bonds plot for G6PD^{Chatham} against G6PD^{WT}

These data suggest that structural changes produced by mutation can influence ligand affinity, subsequently lowering enzyme activity and stability. Meanwhile, the addition of AG1 resulted in the integration of all salt bridges and contributed to the increased stability of AG1 variation. Both hydrogen bonds and salt bridges are crucial in maintaining protein structure—this is consistent with the observed stability of mutant complexes from the RMSD and RMSF experiments. These findings suggest that while mutations may initially impact hydrogen bond formation and salt bridges binding to the AG1 molecule, this molecule significantly increases these interactions.

Radius of Gyration (Rg)

The total compactness of protein during molecular dynamics was determined by calculating the radius of gyration (Rg) of the protein structure. G6PD^{Chatham} had an Rg ranging from 3.75 to 3.60 nm. The Rg reduced to 21 ns and climbed to 36 ns before it increased again to 45 ns. It subsequently stayed constant at 3.67 nm throughout the simulation. Figure 8 depicts the Rg of G6PD^{Chatham} compared to G6PD^{WT} in the presence and absence of AG1. Meanwhile, the variant's fluctuation scores are rated as follows: G6PD^{Chatham} > G6PD$^{Chatham\text{-}AG1}$ > G6PD^{WT}. These data show that mutations alter protein compactness, resulting in enhanced conformational flexibility; however, the protein's compactness was restored upon AG1 binding as exhibited by lower Rg value (see Figure 8b). In summary, the Rg outcomes align with the observations from the RMSD and RMSF analyses. This indicates that GPD^{WT} has a more compact and stable structure than the variants, which may have a more expanding and less stable structure. A smaller Rg value corresponds to a more compact and stable protein conformation, reflecting the tighter packing of atoms around the protein's center of mass. Such compactness is typically associated with a higher density of stabilizing interactions, including hydrogen bonds, hydrophobic interactions, and electrostatic forces, which collectively contribute to the variants' overall stability. Meanwhile, deviations may arise from diverse factors, including mutations within the protein sequence or binding of ligands to specific binding sites, thereby affecting protein folding and stability. Previous studies suggest that a higher Rg value signifies less compactness while a lower Rg value suggests increased compactness and improved stability [59, 60]. This observation strongly implies that the AG1 molecule plays a pivotal role in the folding process of the chosen variant, resulting in enhanced stability and compactness.

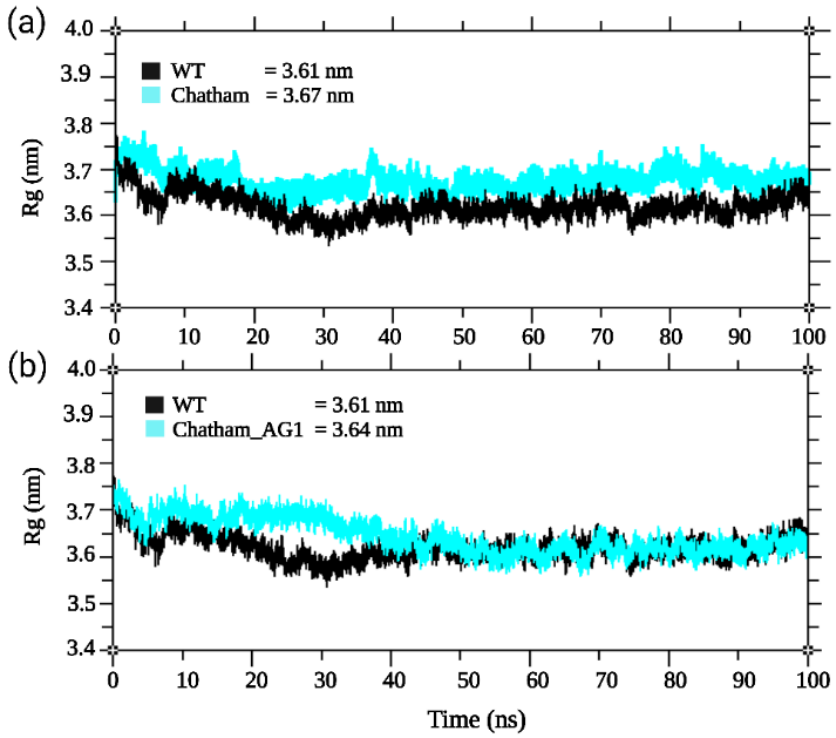

Figure 8. Rg plots during 100 ns simulation displaying the conformational behavior of G6PD^{Chatham} before (a) and after (b) AG1 binding against G6PD^{WT}

Solvent Accessible Surface Area (SASA)

SASA represents the total surface area of a biomolecule that is accessible to a solvent molecule [61]. As shown in Figure 9a, the SASA values for G6PD^{Chatham} and G6PD^{WT} were 431 nm^2 and 416 nm^2, respectively. The substitution of small hydrophobic alanine by polar threonine in G6PD^{Chatham} resulted in higher SASA value compared to G6PD^{WT}. It indicates a possible shift in amino acid residues from the buried region to the accessible region, which then increases its interaction with the solvent. This might lead to conformational changes in the protein structure. Such results agree with the biochemical findings by Gómez-Manzo *et al*. (2014) [62] who reported that class B/II mutant enzymes exhibited rearrangements within their hydrophobic pockets, leading to a shift towards a more solvent-exposed environment. The findings emphasize the intricate link between protein structure, hydrophobic interactions, and stability, emphasizing the need to better understand the molecular mechanisms behind these occurrences.

Furthermore, G6PD^{Chatham_AG1} recorded a decrease in SASA value at 426 nm^2, exhibiting a pattern similar to the native protein (416 nm^2) (see Figure 9b). This suggests a link between reduced interaction with the surrounding solvent. The functional activity of a protein heavily relies on the integrity of its 3D structure, which, in turn, is determined by the proper folding and stability of the polypeptide chain [63]. Changes in SASA values are indicative of the folding and unfolding of the protein complex [61]. Therefore, it can be concluded that the selected variant has a less folded structure compared to G6PD^{WT}. Interestingly, the binding of the AG1 molecule resulted in reduced SASA, implying that AG1 contributes to structural corrections and can potentially lead to more folded structures [61]. This observation suggests that achieving the correct native structure is crucial for the proper functioning of enzyme.

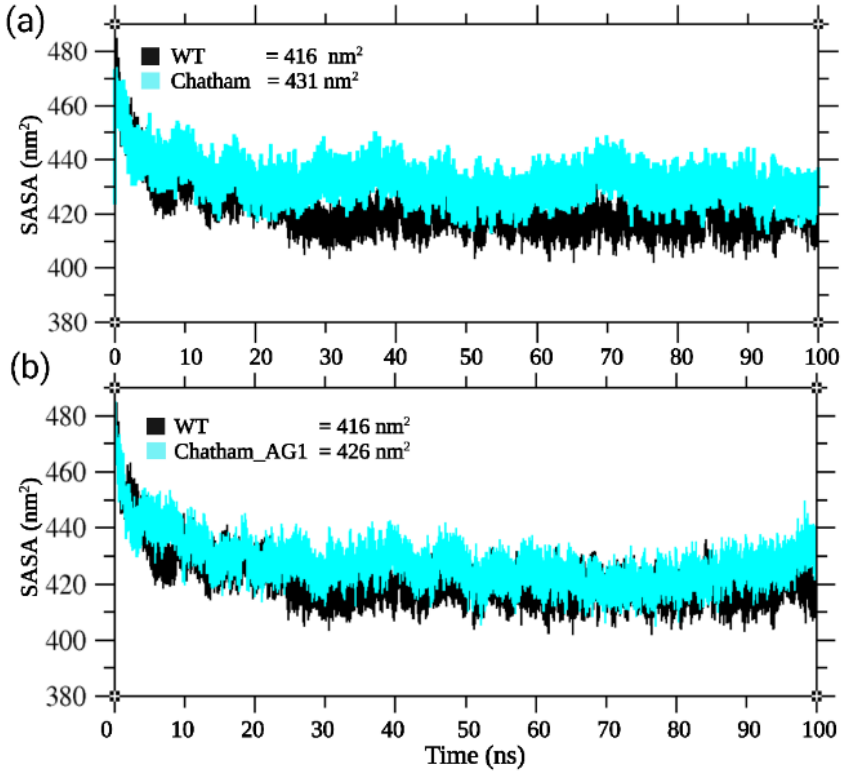

Figure 9. SASA plots of G6PD^{Chatham} before (a) and after (b) AG1 binding against G6PD^{WT} during 100 ns simulation

Covariance Matrix Analysis

The primary purpose of using covariance matrix analysis is to determine the functional collective motion rather than focusing on more localized fluctuations in proteins [64]. A protein's atoms are bound to one another by multiple covalent and non-covalent interactions. The interconnectedness of such huge and complicated network results in correlated structural dynamics, whereby a disturbance or movement of one structural component covaries with the positional displacements of other components [64]. Visual analysis indicated that the wild type atoms primarily displayed associated motions while the red and blue sections represented the positive (correlated) and negative (anti-correlated) motions of the backbone atoms, respectively. Meanwhile, the covariance matrix traces of G6PD^{Chatham} and G6PD^{WT} were 121.515 nm^2 and 91.026 nm^2, respectively. According to Ndagi *et al*. (2017) [65], changes in protein structure are indicated by changes in their associated motion and dynamic patterns. The correlation matrix analysis revealed that G6PD^{Chatham} displayed considerable structural mobility compared to G6PD^{WT}, resulting in a change in structural conformation. It denotes that the G6PD^{WT} atoms were mostly involved in correlated movements than the chosen variation, which demonstrated greater anti-correlated motion. The G6PD^{WT} states appeared to be more compact than the G6PD^{Chatham} states, which had a significantly distorted atomic backbone motion. After AG1 binding, the covariance matrix values for G6PD$^{Chatham\text{-}_AG1}$ and G6PD^{WT} were 105.124 nm^2 and 91.027 nm^2, respectively. Following the AG1 activator binding, G6PD^{Chatham_AG1} exhibited the highest level of correlated motions compared to G6PD^{WT}. It suggests that mutations prior to AG1 binding promoted greater collective global flexibility; however, the variants' flexibility was reduced once the AG1 molecule was bound [19]. This indicates that G6PD^{Chatham_AG1} adopts a more compact conformation compared to G6PD^{WT}. These findings align with the conclusions drawn from the previous analysis.

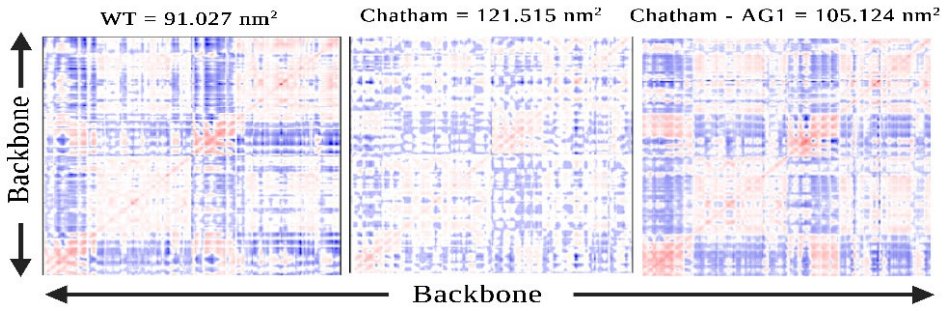

Figure 10. Covariance matrix analysis of G6PD^{Chatham} before and after AG1 binding against G6PD^{WT}

Design of the Activator Molecule

The entire compound of the AG1 molecule consisted of two 2-{[2-(1H-indol-3-yl)ethyl]amino}ethane-1-thiol molecules that were linked by a disulfide linker. Previous docking experiments of Class I/A G6PD variants found that all functional groups play an essential role in the interaction with amino acids at the binding site, except for disulfide linker [19]. Therefore, this group was substituted with various functional groups (1-cyclohexylmethanamine, 1,2-diazinane, 3,4,5,6 tetrahydropyridazine, and 3,4-dihydropyridazine) across SY7, SY8, SY9, and SY10 within the selected variant. Figure 11 shows a 2D structure of the developed molecules.

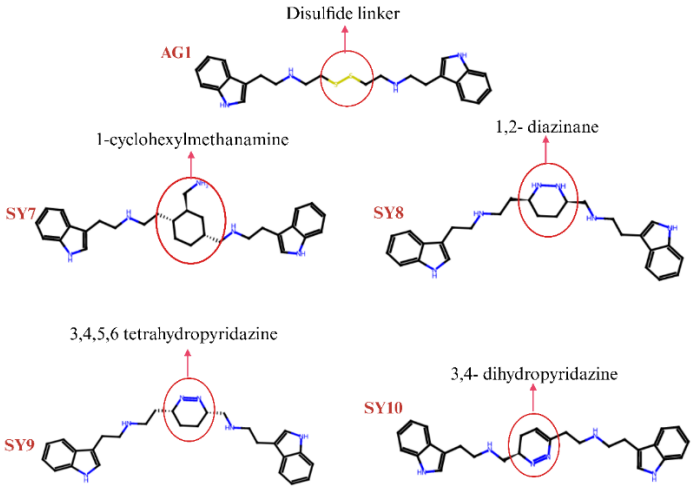

Figure 11. Comparison of 2D structures of SYs models to AG1 activator

Molecular Docking

G6PD^{Chatham} was docked individually with each of the SYs (7–10) molecules. The RMSD/lower and higher bond values for all analogous were zero. The analogous docking results, including the best binding affinity, are summarized in Table 3. Further analysis of the docking results revealed that the best binding affinity fell within the range of (-8.0 to -9.1) kcal/mol (see Figure 12). Moreover, all AG1 analogues were successfully docked at the dimer interface, indicating a consistent docking pattern and comparable binding affinities. Improper ligand binding can cause various side effects in the body, including increased toxicity. Several factors influence these binding affinities, including hydrogen bond donors, hydrophobic or hydrophilic interactions, ionization, and zinc compound chelation [22]. Furthermore, protein binding sites exist primarily for functional reasons, making them important targets for drug design. Most effective medications work by interacting with endogenous small molecules for binding sites on proteins [66]. To be effective, a medicine must have an acceptable potency in binding to its molecular target. This competitive binding is required to alter the protein's activity and achieve the desired therapeutic effect. Therefore, recognizing the interaction between medicines and protein binding sites is critical to create effective medications.

Table 3. The best binding affinity was identified by docking the SYs analogues to G6PD^{Chatham} compared to G6PD^{Chatham_AG1}

G6PD Variants	Best Binding Docking Affinity (kcal/mol)
G6PD^{Chatham_AG1}	-7.1
G6PD^{Chatham_SY7}	-8.0
G6PD^{Chatham_SY8}	-8.8
G6PD^{Chatham_SY9}	-9.1
G6PD^{Chatham_SY10}	-9.1

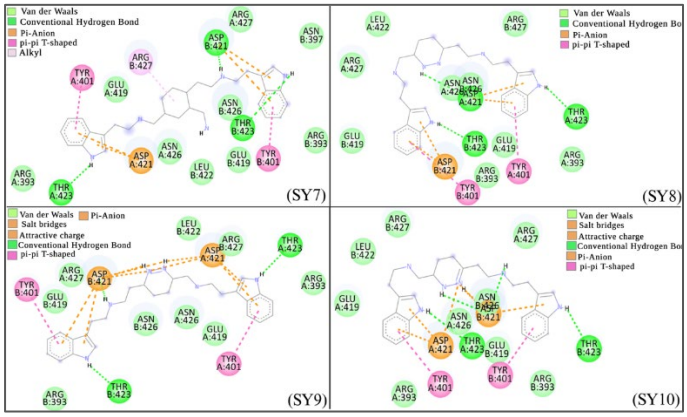

Figure 12. Docking analysis of G6PD^{Chatham} after (SY7, SY8, SY9, and SY10) binding. [SY7, SY8, SY9, and SY10] molecules are represented in 2D line model. Interactions are depicted as dashed lines with circles highlighting the amino acids involved

ADME analysis

A drug's ability to be orally bioavailable is one of the essential properties of drug development [67]. The drug-likeness and pharmacokinetic properties (ADME) of a drug can be predicted prior to an experiment. This information is useful for developing lead molecules as a medication suitable for patient consumption. In this study, the SWISS-ADME server was utilized to predict the drug-likeness and pharmacokinetic properties of the candidate compounds (see Table 4). The Lipinski rule is widely used to characterize the drug-like properties of a candidate drug based on physicochemical properties, including molecular weight (MW) ≤ 500 g/mol, Log P (between 0 to 5), number of hydrogen bond acceptor (HBA ≤ 10) and hydrogen bond donor (HBD ≤ 5), and topological polar surface area (TPSA) ≤ 140Å. The results indicated that all compounds obeyed the Lipinski rule of 5, but a violation was observed in compound SY8 HBD = 6.

Assessment of drug transport across a membrane refers to topological polar surface area (TPSA) < 140 Å^2, indicating good gastrointestinal absorption determined by the Caco-2 monolayer permeability model [68]. This is supported by the GI absorption parameter where all compounds showed high GI absorption, suggesting that these compounds will reach the systematic circulation (bioavailability = 0.55) and are suitable to be administered orally to patients. The principles upheld by the consensus Log P indicate that the compounds have acceptable lipophilicity; hence, they can reach the target (G6PD enzyme) through penetration of the RBC membrane. According to the water solubility parameter (Log S), all designed compounds were determined to be insoluble (AG1 and SY7) and moderately soluble (SY8, SY9, and SY10). P-glycoprotein (P-gp) is a multi-drug resistance protein responsible for transporting drugs out of the cells. All compounds exhibited the characteristics of P-gp substrates, indicating that they will not accumulate inside the cells, which can cause cellular toxicity. Furthermore, these compounds were predicted not to cause neurotoxic effects as indicated by the inability to cross BBB, subsequently implying limited access to the central nervous system (CNS). Inhibition of cytochrome P450 enzymes (CYP) is an indicator of drug metabolism in the body. During the metabolism process, the structure of the drugs is modified to facilitate its elimination and secretion from the body. This is important to eliminate potential toxicity caused by a buildup of drug concentration in the body. Based on the analysis, AG1, SY9 and SY 10 inhibited four out of the five CYP enzymes, suggesting a hindered metabolism process and potentially causing toxicity due to slow excretion from the body. Conversely, SY8 is predicted to be easily metabolized and secreted from the body; hence, it is regarded as the least possible compound to cause toxicity. All compounds exhibited synthetic accessibility of less than 5, indicating that they can be easily synthesized. Overall, SY8 emerged as a promising drug candidate and G6PD activator based on drug-likeness and pharmacokinetic properties. Such compound can also be synthesized for cellular testing. Figure 13 denotes the ADME properties of AG1 and the designed G6PD small activators.

Table 4. Physiochemical properties of AG1 and the designed activators molecules determined by ADME Server

Descriptors	AG1	SY7	SY8	SY9	SY10
Physiochemical Properties					
Formula	$C_{24}H_{30}N_4S_2$	$C_{30}H_{41}N_5$	$C_{27}H_{36}N_6$	$C_{27}H_{34}N_6$	$C_{27}H_{32}N_6$
MW g/mol	438.65	471.68	444.61	442.60 g/mol	440.58 g/mol
No. of heavy atoms	30	35	33	33	33
Num. from. Heavy atoms	18	18	18	18	18
Fraction Csp3	0.33	0.47	0.41	0.41	0.33
No. of rot. bond	13	12	11	11	11
Num. HBA	2	3	4	4	4
Num. HBD	4	5	6	4	4
Molecular reactivity	134.04	148.30	144.60	142.68	142.20
tPSA (Å²)	106.24	81.66	79.70	80.36	80.36
Lipophilicity					
Consensus Log Po/w	4.47	4.65	3.49	4.40	4.42
Water Solubility					
Log S (ESOL)	-4.80	-5.35	-4.70	-5.08	-5.08
Class	Insoluble	Insoluble	Insoluble	Insoluble	Insoluble
Pharmacokinetics					
GI absorption	High	High	High	High	High
BBB permeant	No	No	No	No	No
P-gp substrate	Yes	Yes	Yes	Yes	Yes
CYP1A2 inhibitor	Yes	Yes	No	No	No
CYP2C19 inhibitor	Yes	Yes	Yes	Yes	Yes
CYP2C9 inhibitor	No	No	No	Yes	Yes
CYP2D6 inhibitor	Yes	No	No	Yes	Yes
CYP3A4 inhibitor	Yes	Yes	Yes	Yes	Yes
Drug likeness					
Lipinski	Yes; 0 violation	Yes; 0 violation	Yes; 1 violation: NHorOH>5	Yes; 0 violation	Yes; 0 violation
Bioavailability Score	0.55	0.55	0.55	0.55	0.55
Medicinal Chemistry					
PAINS	0 alert	0 alert	0 alert	0 alert	0 alert
Brenk	1 alert: disulphide	0 alert	0 alert	0 alert	0 alert
Lead likeness	No; 3 violations: MW>350, Rotors>7, XLOGP3>3.5	No; 3 violations: MW>350, Rotors>7, XLOGP3>3.5	No; 3 violations: MW>350, Rotors>7, XLOGP3>3.5	No; 3 violations: MW>350, Rotors>7, XLOGP3>3.5	No; 3 violations: MW>350, Rotors>7, XLOGP3>3.5
Synthetic accessibility	3.17	4.28	4.29	4.35	4.73

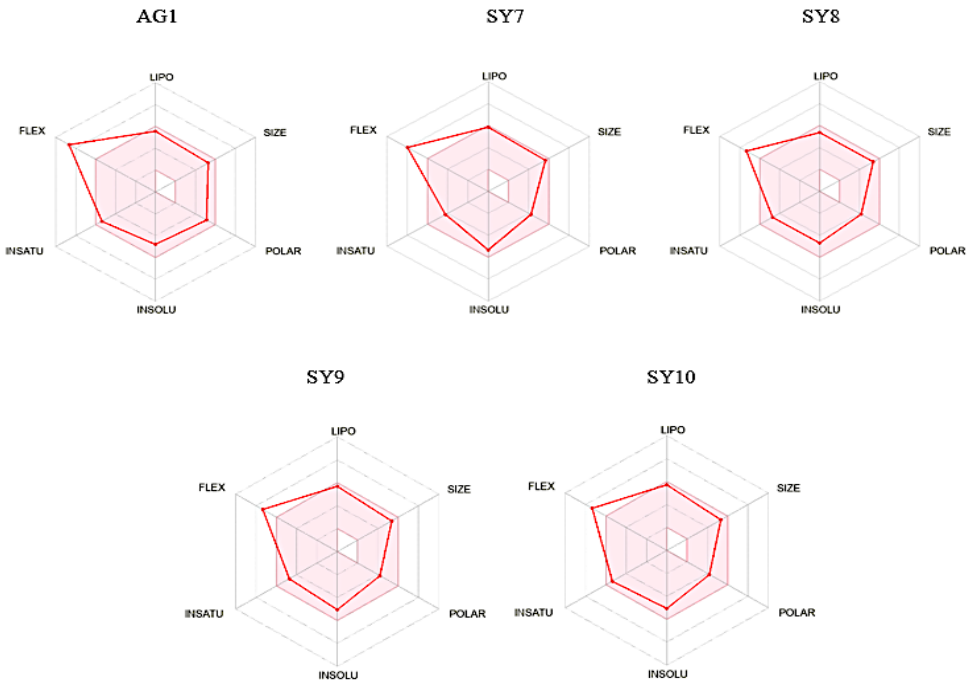

Figure 13. ADME properties of AG1 and the designed G6PD small molecule activators (SY7, SY8, SY9, and SY10). The pink area represents the optimal range for each property (lipophilicity: XLOGP3 between ne−0.7 and +5.0, size: MW between 150 and 500 g/mol, polarity: TPSA between 20 and 130Å2, solubility: log S not higher than 6, saturation: fraction of carbons in sp3 hybridization not less than 0.25, and flexibility: no more than 9 rotatable bonds)

A number of parameters, such as mutagenicity, tumorigenicity, irritant, and reproductive risk, were calculated to assess toxicity. The Osiris toxicity risk predictor recognizes fragments inside a molecule, which indicates a potential toxicity risk. Findings from the toxicity risk assessment revealed that chemicals AG1, SY7, and SY8 posed no danger of mutagenicity, tumorigenicity, irritant, or reproductive toxicity while the SY9 and SY10 molecules were strongly mutagenic and tumorigenic with a moderate level of tumorigenicity and irritant (see Table 5). The overall drug score was generated to determine the overall drug potential, which incorporated drug-likeness, hydrophilicity (cLogP), aqueous solubility (LogS), MW, and toxicity risk characteristics. The LogP value was expected to assess the hydrophilicity of all chemicals while both SY9 and SY10 had substantial restrictions. Overall, SY8 emerged as the best potential drug candidate due to its high drug score, strong drug-likeness, and safety profile. AG1 and SY7 are also acceptable choices, although SY9 and SY10 have considerable drawbacks (see Figure 14). These findings provide an overall drug score with anticipated active chemicals, which adds confidence in the discovery of additional G6PD small-molecule activators for G6PD deficient disorders.

Table 5. The ADMET characteristics of AG1 and the four designed molecules that were computed using the Osiris Molecular Property Explorer

Categories	AG1	SY7	SY8	SY9	SY10
Properties	No	No	No	Moderate	Moderate
Mutagenic	No	No	No	High	High
Tumorigenic	No	No	No	Moderate	No
Irritant	No	No	No	Moderate	No
Reproductive effect	No	No	No	No	No
cLogP	4.22	3.82	2.04	2.81	2.89
Solubility	-5.18	-5.38	-5.01	-5.06	-5.19
MW	438	471	444	442	440
TPSA	106.2	81.66	79.7	80.36	80.36
Drug likeness	1.76	1.47	2.49	- 2.76	-1.29
Drug score	0.48	0.45	0.58	0.12	0.17

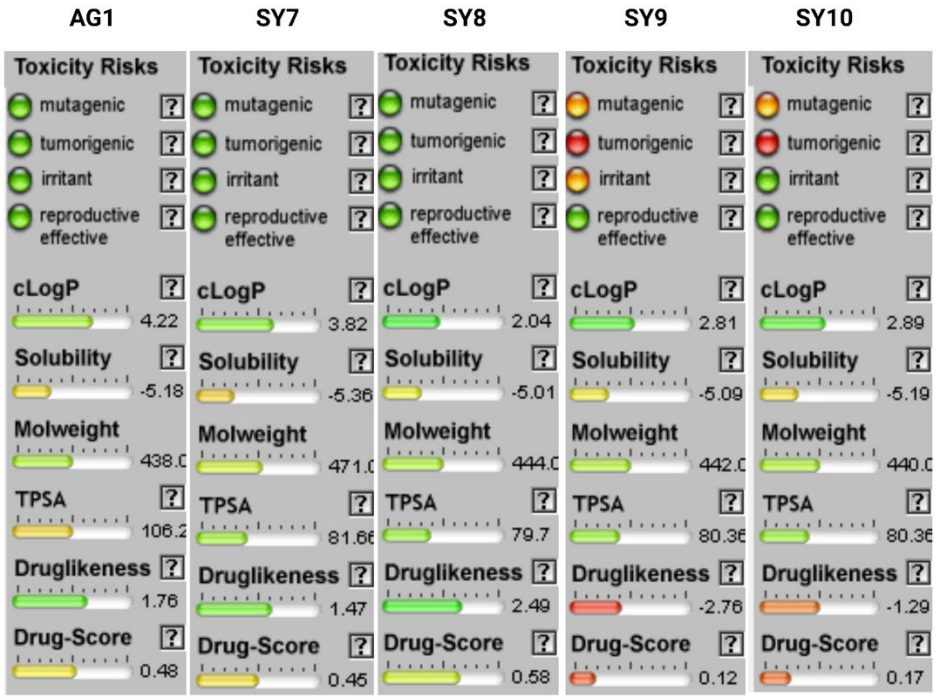

Figure 14. Toxicity prediction of AG1 and the designed molecules (SY7, SY8, SY9, and SY10) was performed using the online Molecular Properties Prediction Server, Osiris Property Explorer. High-risk properties are shown in red, green indicates low risk, and yellow signifies medium risk

Based on the ADME analysis and toxicity risk assessment, SY8 emerged as the best possible medication candidate, despite SY9 and SY10 having the highest binding affinity. This is due to a protein's capacity to bind small molecules with the required chemical characteristics and binding affinity may make it druggable; nevertheless, it does not necessarily make it a possible drug target. Thus, understanding how to distinguish between drug ability and drug target helps facilitate drug development by focusing on proteins that can bind medications while performing a key role in disease development.

Conclusion

G6PDD is a frequent enzymopathy in humans that results from point mutations and causes severe deficiency. Despite its widespread effect, no medications are currently available to treat G6PDD. The present research on the G6PD^{Chatham} mutation sheds light on the reasons for the severity of AHA-related conditions by examining the molecular foundation underlying the variant structure. G6PD^{Chatham} has significant structural distinctions from the wild type, involving the breaking of hydrogen bonds and salt bridge interactions, which might affect overall stability and exacerbate G6PDD severity. Addressing these defects is critical and this study found promising evidence in repairing them by adding missing interactions through AG1 docking at the dimer interface, resulting in a highly stable structure. Moreover, the addition of AG1 molecules can improve G6PD dimerization into an enzymatically functional state, hence lowering dynamic fluctuations and stabilizing variants. Clarifying these molecular pathways can provide a better understanding of the correlation between G6PD mutation and the severity of related disorders, such as AHA. Several new molecules originating from the AG1 molecule were produced by replacing the SS linker with different functional groups to develop G6PD activators for treating G6PDD. SY8 is predicted to be easily metabolized and excreted, making it the least likely candidate to cause toxicity. All compounds showed a synthetic accessibility score of less than 5, indicating ease of synthesis. SY8 stands out as a promising G6PD activator based on its drug-like and pharmacokinetic properties, making it a strong candidate for synthesis and cellular testing. Its high drug score, strong drug-likeness, and favorable safety profile further enhance its potential. In contrast, SY9 and SY10 have considerable drawbacks. The toxicity risk assessment supported the overall drug score, increasing confidence in discovering additional G6PD small-molecule activators for G6PDD disorders. The structural characterization revealed details about their physicochemical properties and possible pharmacological effects, subsequently establishing a structure for future study in both clinical and preclinical settings. This

information is promising for enhancing the lives of those with AHA and helps in the development of suited medicines for G6PDD. Future research can improve the study's dependability by validating computational predictions. This includes investigating the stability and dynamic behavior of the analogue's complexes by running 100 ns of MDS alongside conducting laboratory investigations, such as enzyme kinetics and activity assays, on variants with distinct structural features.

Conflicts of Interest

The author(s) declare(s) that there is no conflict of interest regarding the publication of this paper.

Acknowledgement

This work was supported by the Intramural Research Fund awarded by Ministry of Health, Kingdom of Saudi Arabia (IRF Grant # 018-066).

References

[1] Helegbe, G. K., *et al.* (2023). Co-occurrence of G6PD deficiency and SCT among pregnant women exposed to infectious diseases. *Journal of Clinical Medicine, 12*(15), 1–14. https://doi.org/10.3390/jcm12155085

[2] Wei, H., *et al.* (2023). Simultaneous detection of G6PD mutations using SNPscan in a multiethnic minority area of Southwestern China. *Frontiers in Genetics, 13*, 1–10. https://doi.org/10.3389/fgene.2022.1000290

[3] Gandomani, M. G., Khatami, S. R., Nezhad, S. R. K., Daneshmand, S., & Mashayekhi, A. (2011). Molecular identification of G6PD Chatham (G1003A) in Khuzestan Province of Iran. *Journal of Genetics, 90*(1), 143–145. https://doi.org/10.1007/s12041-011-0024-7

[4] Liang, H. F., *et al.* (2023). Molecular epidemiological investigation of G6PD deficiency in Yangjiang region, western Guangdong province. *Frontiers in Genetics, 14*, 1–7. https://doi.org/10.3389/fgene.2023.1345537

[5] Notaro, R., Afolayan, A., & Luzzatto, L. (2000). Human mutations in glucose 6-phosphate dehydrogenase reflect evolutionary history. *FASEB Journal, 14*(3), 485–490. https://doi.org/10.1096/fasebj.14.3.485

[6] Roper, D., *et al.* (2020). Laboratory diagnosis of G6PD deficiency: A British Society for Haematology guideline. *British Journal of Haematology*, 1–15. https://doi.org/10.1111/bjh.16366

[7] Policy, M., & Group, A. (2022). Technical consultation to review the classification of glucose-6-phosphate dehydrogenase (G6PD). Malaria Policy Advisory Group meeting. *World Health Organization Malaria Policy Advisory Group Meeting*, 20.

[8] Malik, S., Zaied, R., Syed, N., Jithesh, P., & Al-Shafai, M. (2021). Seven novel glucose-6-phosphate dehydrogenase (G6PD) deficiency variants identified in the Qatari population. *Human Genomics, 15*(1), 1–10. https://doi.org/10.1186/s40246-021-00358-9

[9] Doss, C. G. P., *et al.* (2016). Genetic epidemiology of glucose-6-phosphate dehydrogenase deficiency in the Arab world. *Scientific Reports*, 1–11. https://doi.org/10.1038/srep37284

[10] Haloui, S., *et al.* (2016). Molecular identification of Gd A- and Gd B-G6PD deficient variants by ARMS-PCR in a Tunisian population. *Annales de Biologie Clinique (Paris), 72*(2), 219–226. https://doi.org/10.1684/abc.2016.1123

[11] Gómez-Manzo, S., *et al.* (2015). Mutations of glucose-6-phosphate dehydrogenase Durham, Santa-Maria, and A+ variants are associated with loss of functional and structural stability of the protein. *International Journal of Molecular Sciences, 16*(12), 28657–28668. https://doi.org/10.3390/ijms161226124

[12] Martínez-Rosas, V., *et al.* (2020). Effects of single and double mutants in human glucose-6-phosphate dehydrogenase variants present in the Mexican population: Biochemical and structural analysis. *International Journal of Molecular Sciences, 21*(8). https://doi.org/10.3390/ijms21082732

[13] Zhou, X., Qiang, Z., Zhang, S., Zhou, Y., Xiao, Q., & Tan, G. (2024). Evaluating the relationship between clinical G6PD enzyme activity and gene variants. *PeerJ, 12*, 1–11. https://doi.org/10.7717/peerj.16554

[14] Siderius, M., & Jagodzinski, F. (2018). Mutation sensitivity maps: Identifying residue substitutions that impact protein structure via a rigidity analysis in silico mutation approach. *Journal of Computational Biology, 25*(1), 89–102. https://doi.org/10.1089/cmb.2017.0165

[15] Siler, U., *et al.* (2017). Severe glucose-6-phosphate dehydrogenase deficiency leads to susceptibility to infection and absent NETosis. *Journal of Allergy and Clinical Immunology, 139*(1), 212–219.e3. https://doi.org/10.1016/j.jaci.2016.04.041

[16] Alakbaree, M., *et al.* (2023). G6PD deficiency: Exploring the relationship with different medical disorders. *Journal of Contemporary Medical Sciences, 9*(5). https://doi.org/10.22317/jcms.v9i5.1433

[17] Luzzatto, L., Ally, M., & Notaro, R. (2021). Glucose-6-phosphate dehydrogenase deficiency. *Blood, 136*(11), 1225–1240. https://doi.org/10.1182/blood.2019000944

[18] Raub, A. G., *et al.* (2019). Small-molecule activators of glucose-6-phosphate dehydrogenase (G6PD) bridging the dimer interface. *ChemMedChem, 14*(14), 1321–1324. https://doi.org/10.1002/cmdc.201900341

[19] Alakbaree, M., *et al.* (2023). A computational study of structural analysis of Class I human glucose-6-phosphate dehydrogenase (G6PD) variants: Elaborating the correlation to chronic non-spherocytic hemolytic anemia (CNSHA). *Computational Biology and Chemistry, 104*. https://doi.org/10.1016/j.compbiolchem.2023.107873

[20] Salman, M. M., Al-Obaidi, Z., Kitchen, P., Loreto, A., Bill, R. M., & Wade-Martins, R. (2021). Advances in

applying computer-aided drug design for neurodegenerative diseases. *International Journal of Molecular Sciences, 22*(9).

[21] Pathak, R. K., Singh, D. B., Sagar, M., Baunthiyal, M., & Kumar, A. (2020). Computational approaches in drug discovery and design. In *Computational Drug Design* (pp. 1–21). https://doi.org/10.1007/978-981-15-6815-2_1

[22] Opo, F. A. D. M., Rahman, M. M., Ahammad, F., Ahmed, I., Bhuiyan, M. A., & Asiri, A. M. (2021). Structure-based pharmacophore modeling, virtual screening, molecular docking and ADMET approaches for identification of natural anti-cancer agents targeting XIAP protein. *Scientific Reports, 11*(1), 1–17. https://doi.org/10.1038/s41598-021-83626-x

[23] Sams-Dodd, F. (2005). Target-based drug discovery: Is something wrong? *Drug Discovery Today, 10*(2), 139–147. https://doi.org/10.1016/S1359-6446(04)03316-1

[24] Fiorelli, G., & Martinez, F. (2000). Chronic non-spherocytic haemolytic disorders associated with glucose-6-phosphate dehydrogenase variants. *British Journal of Haematology, 13*(1), 39–55. https://doi.org/10.1053/beha.1999.0056

[25] Rani, S., Malik, F. P., Anwar, J., & Paracha, R. Z. (2022). Investigating the effect of mutation on structure and function of G6PD enzyme: A comparative molecular dynamics simulation study. *PeerJ*. https://doi.org/10.7717/peerj.12984

[26] Alakbaree, M., *et al.* (2022). Construction of a complete human glucose-6-phosphate dehydrogenase dimer structure bound to glucose-6-phosphate and nicotinamide adenine dinucleotide phosphate cofactors using molecular docking approach. In *AIP Conference Proceedings, 2394*. https://doi.org/10.1063/5.0121720

[27] Stanzione, F., Giangreco, I., & Cole, J. C. (2021). Use of molecular docking computational tools in drug discovery (1st ed., Vol. 60). Elsevier B.V. https://doi.org/10.1016/bs.pmch.2021.01.004

[28] Wang, J., Cao, D., Tang, C., Chen, X., Sun, H., & Hou, T. (2020). Fast and accurate prediction of partial charges using atom-path-descriptor-based machine learning. *Bioinformatics*, 1–8. https://doi.org/10.1093/bioinformatics/btaa566

[29] Adeniji, S. E., Arthur, D. E., Abdullahi, M., & Haruna, A. (2020). Quantitative structure–activity relationship model, molecular docking simulation and computational design of some novel compounds against DNA gyrase receptor. *Chemistry Africa, 3*(2), 391–408. https://doi.org/10.1007/s42250-020-00132-9

[30] Baba Muh'd, M., Uzairu, A., Shallangwa, G. A., & Uba, S. (2020). Molecular docking and quantitative structure-activity relationship study of anti-ulcer activity of quinazolinone derivatives. *Journal of King Saud University - Science, 32*(1), 657–666. https://doi.org/10.1016/j.jksus.2018.10.003

[31] O'Boyle, E. H. Jr., Humphrey, R. H., Pollack, J. M., Hawver, T. H., & Story, P. A. (2011). The relation between emotional intelligence and job performance: A meta-analysis. *Journal of Organizational Behavior, 32*(5), 788–818.

[32] Trott, O., & Olson, A. J. (2010). AutoDock Vina: Improving the speed and accuracy of docking with a new scoring function, efficient optimization, and multithreading. *Journal of Computational Chemistry*.

[33] Roy, K., Kar, S., & Das, R. N. (2015). Other related techniques. https://doi.org/10.1016/b978-0-12-801505-6.00010-7

[34] Jokhakar, P. H., Kalaria, R., & Patel, H. K. (2020). In silico docking studies of antimalarial drug hydroxychloroquine to SARS-CoV proteins: An emerging pandemic worldwide. https://doi.org/10.26434/chemrxiv.12488804.v1

[35] Abraham, M., Hess, B., van der Spoel, D., & Lindahl, E. (2015). Gromacs 5.0.7. *SpringerReference*. https://doi.org/10.1007/SpringerReference_28001

[36] Schmid, N., *et al.* (2011). Definition and testing of the GROMOS force-field versions 54A7 and 54B7. *European Biophysics Journal, 40*(7), 843–856. https://doi.org/10.1007/s00249-011-0700-9

[37] Singh, V., Dhankhar, P., Dalal, V., Tomar, S., & Kumar, P. (2022). In-silico functional and structural annotation of hypothetical protein from Klebsiella pneumonia: A potential drug target. *Journal of Molecular Graphics and Modelling, 116*, 108262. https://doi.org/10.1016/j.jmgm.2022.108262

[38] Kaushik, S., Rameshwari, R., & Chapadgaonkar, S. S. (2024). The in-silico study of the structural changes in the *Arthrobacter globiformis* choline oxidase induced by high temperature. *Journal of Genetic Engineering and Biotechnology, 22*(1), 100348. https://doi.org/10.1016/j.jgeb.2023.100348

[39] Kumar, H., & Maiti, P. K. (2011). Introduction to molecular dynamics simulation. *pp.* 161–197. https://doi.org/10.1007/978-93-86279-50-7_6

[40] Alamri, M. A., ul Qamar, M. T., Afzal, O., Alabbas, A. B., Riadi, Y., & Alqahtani, S. M. (2021). Discovery of anti-MERS-CoV small covalent inhibitors through pharmacophore modeling, covalent docking, and molecular dynamics simulation. *Journal of Molecular Liquids, 330*, 115699.

[41] Hanwell, M. D., Curtis, D. E., Lonie, D. C., Vandermeerschd, T., Zurek, E., & Hutchison, G. R. (2012). Avogadro: An advanced semantic chemical editor, visualization, and analysis platform. *Journal of Cheminformatics, 4*(8). https://doi.org/10.1186/1758-2946-4-17

[42] Daina, A., Michielin, O., & Zoete, V. (2017). SwissADME: A free web tool to evaluate pharmacokinetics, drug-likeness and medicinal chemistry friendliness of small molecules. *Scientific Reports, 7*, 42717. https://doi.org/10.1038/srep42717

[43] Bhal, S. K. (2007). Log P — Making sense of the value. *Advances in Chemical Development*, 1–4. www.acdlabs.com/logp

[44] Minucci, A., Moradkhani, K., Jing, M., Zuppi, C., Giardina, B., & Capoluongo, E. (2012). Blood cells, molecules, and diseases glucose-6-phosphate dehydrogenase (G6PD) mutations database: Review of the 'old' and update of the new mutations. *Blood Cells, Molecules, and Diseases, 48*(3), 154–165. https://doi.org/10.1016/j.bcmd.2012.01.001

[45] Sirdah, M., *et al.* (2012). Molecular heterogeneity of glucose-6-phosphate dehydrogenase deficiency in Gaza Strip Palestinians. *Blood Cells, Molecules, and Diseases, 49*(3–4), 152–158. https://doi.org/10.1016/j.bcmd.2012.06.003

[46] Čalyševa, J., & Vihinen, M. (2017). PON-SC - program for identifying steric clashes caused by amino acid

substitutions. *BMC Bioinformatics, 18*(1), 1–8. https://doi.org/10.1186/s12859-017-1947-7

[47] Alakbaree, M., *et al*. (2022). Human G6PD variant structural studies: Elucidating the molecular basis of human G6PD deficiency. *Gene Reports, 27*. https://doi.org/10.1016/j.genrep.2022.101634

[48] Doering, J. A., *et al*. (2018). In silico site-directed mutagenesis informs species-specific predictions of chemical susceptibility derived from the sequence alignment to predict across species susceptibility (SeqAPASS) tool. *Toxicological Sciences, 166*(1), 131–145. https://doi.org/10.1093/toxsci/kfy186

[49] Studio, D., & . (2008). Discovery Studio Life Science Modeling and Simulations. *ResearchGate*. https://www.researchgate.net/profile/Tanweer_Alam8/post/hi_can_somebody_plz_tell_me_how_to_import_a_database_into_Discovery_Studio_for_a_3D_database_search/attachment/59d63bb879197b8077998bbd/AS%3A412232203685889%401475295224962/download/ds-overview-20.pd

[50] Lemkul, J. (2019). From proteins to perturbed hamiltonians: A suite of tutorials for the GROMACS-2018 molecular simulation package [Article v1.0]. *Living Journal of Computational Molecular Science, 1*(1), 1–53. https://doi.org/10.33011/livecoms.1.1.5068

[51] Praoparotai, A., Junkree, T., Imwong, M., & Boonyuen, U. (2020). Functional and structural analysis of double and triple mutants reveals the contribution of protein instability to clinical manifestations of G6PD variants. *International Journal of Biological Macromolecules, 158*, 884–893. https://doi.org/10.1016/j.ijbiomac.2020.05.026

[52] Kumar, A., & Purohit, R. (2013). Cancer associated E17K mutation causes rapid conformational drift in AKT1 pleckstrin homology (PH) domain. *PLoS One, 8*(5), 1–10. https://doi.org/10.1371/journal.pone.0064364

[53] Sukumar, S., Mukherjee, M. B., Colah, R. B., & Mohanty, D. (2003). Molecular characterization of G6PD Insuli — a novel 989 CGC 3 CAC (330 Arg 3 His) mutation in the Indian population. *Molecular Medicine, 30*, 246–247. https://doi.org/10.1016/S1079-9796(03)00018-4

[54] Au, S. W. N., Gover, S., Lam, V. M. S., & Adams, M. J. (2000). Human glucose-6-phosphate dehydrogenase: The crystal structure reveals a structural NADP+ molecule and provides insights into enzyme deficiency. *Structure, 8*(3), 293–303. https://doi.org/10.1016/S0969-2126(00)00104-0

[55] Kumar, S., & Nussinov, R. (1999). Salt bridge stability in monomeric proteins. *Journal of Molecular Biology, 293*(5), 1241–1255. https://doi.org/10.1006/jmbi.1999.3218

[56] Li, Z., *et al*. (2023). Genotypic and phenotypic characterization of glucose-6-phosphate dehydrogenase (G6PD) deficiency in Guangzhou, China. *Human Genomics, 17*(1), 1–11. https://doi.org/10.1186/s40246-023-00473-9

[57] Sen Gupta, P. S., Mondal, S., Mondal, B., Ul Islam, R. N., Banerjee, S., & Bandyopadhyay, A. K. (2014). SBION: A program for analyses of salt-bridges from multiple structure files. *Bioinformation, 10*(3), 164–166. https://doi.org/10.6026/97320630010164

[58] Kumar, C. V., Swetha, R. G., Ramaiah, S., & Anbarasu, A. (2015). Tryptophan to glycine mutation in the position 116 leads to protein aggregation and decreases the stability of the LITAF protein. *Journal of Biomolecular Structure and Dynamics, 33*(8), 1695–1709. https://doi.org/10.1080/07391102.2014.968211

[59] Joshi, T., Joshi, T., Sharma, P., Chandra, S., & Pande, V. (2020). Molecular docking and molecular dynamics simulation approach to screen natural compounds for inhibition of *Xanthomonas oryzae* pv. *Oryzae* by targeting peptide deformylase. *Journal of Molecular Graphics and Modelling*. https://doi.org/10.1080/07391102.2020.1719200

[60] Rampadarath, A., Balogun, F. O., Pillay, C., & Sabiu, S. (2022). Identification of flavonoid C-glycosides as promising antidiabetics targeting protein tyrosine phosphatase 1B. *Journal of Diabetes Research, 2022*, 6233217. https://doi.org/10.1155/2022/6233217

[61] Ghahremanian, S., Rashidi, M. M., Raeisi, K., & Toghraie, D. (2022). Molecular dynamics simulation approach for discovering potential inhibitors against SARS-CoV-2: A structural review. *Journal of Molecular Liquids, 354*, 118901. https://doi.org/10.1016/j.molliq.2022.118901

[62] Gómez-Manzo, S., *et al*. (2014). The stability of G6PD is affected by mutations with different clinical phenotypes. *International Journal of Molecular Sciences, 15*(11), 21179–21201. https://doi.org/10.3390/ijms151121179

[63] Masson, P., & Lushchekina, S. (2022). Conformational stability and denaturation processes of proteins investigated by electrophoresis under extreme conditions. *Molecules, 27*(20). https://doi.org/10.3390/molecules27206861

[64] Agrahari, A. K., Sneha, P., George Priya Doss, C., Siva, R., & Zayed, H. (2018). A profound computational study to prioritize the disease-causing mutations in PRPS1 gene. *Metabolic Brain Disease, 33*(2), 589–600. https://doi.org/10.1007/s11011-017-0121-2

[65] Ndagi, U., Mhlongo, N. N., & Soliman, M. E. (2017). The impact of Thr91 mutation on c-Src resistance to UM-164: Molecular dynamics study revealed a new opportunity for drug design. *Molecular Biosystems, 13*(6), 1157–1171. https://doi.org/10.1039/c6mb00848h

[66] Drews, J. (2000). Drug discovery: A historical perspective. *Science, 287*(5460), 1960–1964. https://doi.org/10.1126/science.287.5460.1960

[67] Okolo, E. N., *et al*. (2021). New chalcone derivatives as potential antimicrobial and antioxidant agents. *Scientific Reports, 11*(1), 1–13. https://doi.org/10.1038/s41598-021-01292-5

[68] Sadgir, N. V., Adole, V. A., Dhonnar, S. L., & Jagdale, B. S. (2023). Synthesis and biological evaluation of coumarin appended thiazole hybrid heterocycles: Antibacterial and antifungal study. *Journal of Molecular Structure, 1293*, 136229. https://doi.org/10.1016/j.molstruc.2023.136229